COMMUNICATIONS CHEMISTRY

ARTICLE

DOI: 10.1038/s42004-018-0053-8 OPEN

Profiling the short-lived cationic species generated during catalytic dehydration of short-chain alcohols

Fangjun Wang[1], Zheyi Liu[1] & Guofeng Weng[1]

Short-chain alcohols are important products of biomass conversion and can be further converted into platform chemicals via catalytic dehydration. Although cationic species are believed to be intermediates in the alcohol-to-hydrocarbon processes, directly observing them is still a challenge due to the lack of efficient tools to deal with their instability and short lifetimes. Here we integrate a micro catalytic reactor onto the ion inlet of an Orbitrap mass spectrometer for high-speed, high-sensitivity, and high-throughput detection of the short-lived cationic species generated during dehydration of short-chain alcohols over heterogeneous catalysts. Hundreds of cationic species can be feasibly observed within the catalytic alcohol dehydration on acidic zeolites H-Beta and H-ZSM5. It is demonstrated that these cationic species may feasibly reveal the catalytic reaction activity and selectivity. This strategy has the potential to inform catalyst development and to help refine reaction conditions in the future.

[1] CAS Key Laboratory of Separation Sciences for Analytical Chemistry, National Chromatographic R&A Center, Dalian Institute of Chemical Physics, Chinese Academy of Sciences, Dalian, Liaoning 116023, China. Correspondence and requests for materials should be addressed to F.W. (email: wangfj@dicp.ac.cn)

Detecting the short-lived active species generated within chemical reactions plays crucial roles in elucidating the mechanisms of chemical reactions, discovering new reactions, and screening catalysts[1–4]. Currently, the most popular techniques for active species detection in heterogeneous catalysis are infrared spectroscopy[5], solid-state nuclear magnetic resonance (NMR)[6], electron paramagnetic spectroscopy[7], ultraviolet/visible spectroscopy, and Raman spectroscopy[8,9], which can monitor in situ the generation and dynamic changes of active sites and species on the solid surface.

Cationic species are believed to be involved in many important chemical reactions, such as the heterogeneous catalysis of alcohols to hydrocarbons[10,11]. However, there is still a lack of efficient methods for directly observing these cationic species due to their relatively low abundance and extremely short lifetimes. Generally, an efficient technique for the detection of these short-lived cationic species should be fast and sensitive enough to detect them before their decomposition and capable of high-throughput screening to deal with their complexity.

Mass spectrometry (MS) is extremely useful in active species detection owing to its high sensitivity and high throughput. MS-based strategies usually involve transferring the active species into the gas phase within the MS detector, as well as ionizing the neutral compounds by electrospray ionization or desorption electrospray ionization strategies[12–14]. Many important intermediates generated within homogeneous chemical reaction systems have been successfully detected by MS in recent years, such as essential intermediates in the Pomeranz–Fritsch synthesis of isoquinoline[15] and the reductive amination of 4-pyridinecarboxaldehyde with 4-aminomethyl-pyridine[16]. However, few MS-based strategies have paid attention to detecting the short-lived ionic species natively generated in heterogeneous catalysis with solid-phase catalysts, such as dehydration of short-chain alcohols to platform chemicals[3,17,18].

In this study, we develop a novel strategy for profiling short-lived cationic species by integrating a micro catalytic reactor packed with a solid catalyst onto the ion inlet of an Orbitrap MS (Fig. 1 and Supplementary Figure 1). All gas-phase cationic species generated in the heterogeneous catalysis of short-chain alcohol dehydration can simultaneously come into the MS detector for fast and high-throughput detection without separation, ionization, or any other perturbation steps. Then, hundreds of cationic species are directly observed during the catalytic alcohol dehydration on acidic zeolites and these cationic species are demonstrated to be directly related to the catalytic activity and selectivity.

Results

Butanol dehydration on γ-Al_2O_3. To demonstrate the efficiency of our new strategy in discovering the short-lived cationic species, heterogeneous catalysis of butanol dehydration on weak acidic γ-Al_2O_3 was investigated. First, 1-butanol was injected into the micro catalytic reactor packed with γ-Al_2O_3 and the reaction temperature was controlled at 373 K. It was observed that the most abundant cationic species was 1-butanol with sodium ions $[C_4H_{10}ONa]^+$ (Supplementary Figure 2 and Supplementary Data 1). Then, the reaction temperature of the micro catalytic reactor was increased to 423 K and three cationic species began to appear with the elemental composition $[(C_4H_{10}O)_2H]^+$, $[(C_4H_9)_2OH]^+$, and $[C_4H_9]^+$, which might belong to the protonated 1-butanol dimer, protonated 1-butanol ether, and 1-butanol dehydration cationic species, respectively (Fig. 2a, Supplementary Figure 2, and Supplementary Data 1). The abundances of these three cationic species grew exponentially along with the increase of catalytic reaction temperature from 423 to 723 K (Supplementary Figure 2). Obviously, the $[(C_4H_{10}O)_2H]^+$ is one of the most abundant cationic species generated during the heterogeneous catalysis of 1-butanol dehydration, even higher than the 1-butanol molecular ion at 723 K, demonstrating that the protonated 1-butanol dimers widely existed in this heterogeneous catalysis system. If we remove γ-Al_2O_3 catalyst and inject 1-butanol into a void reactor, only the butanol molecular ion $[C_4H_{10}ONa]^+$ was clearly observed at 723 K, and the abundances of the other three cationic species were all decreased over two orders of magnitude (Supplementary Figure 3). Thus, the cationic species $[(C_4H_{10}O)_2H]^+$, $[(C_4H_9)_2OH]^+$, and $[C_4H_9]^+$ are indeed involved in the γ-Al_2O_3 catalytic 1-butanol dehydration.

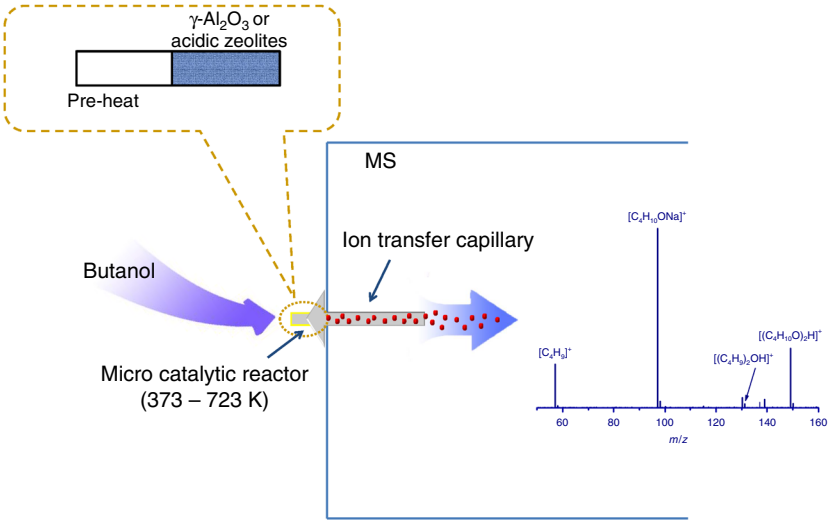

Fig. 1 Schematic diagram of cationic species detection. The micro catalytic reactor with a reaction chamber (1 mm i.d. × 8 mm) packed with γ-Al_2O_3 or acidic zeolites (H-Beta or H-ZSM5) was integrated onto the inlet of ion transfer capillary of an Orbitrap XL MS (Thermo) and kept at an appropriate reaction temperature (373–723 K). The injected alcohol was heated, gasified, and passed through the solid-phase catalyst as the inside of MS was maintained in high vacuum. Finally, all of the gas-phase cationic species generated in the catalytic reaction were simultaneously transferred into the MS detector without any perturbation steps. The system pressure was about 100 Pa during the catalytic reaction. No ionization voltage (0 V) was applied to the MS during the whole process

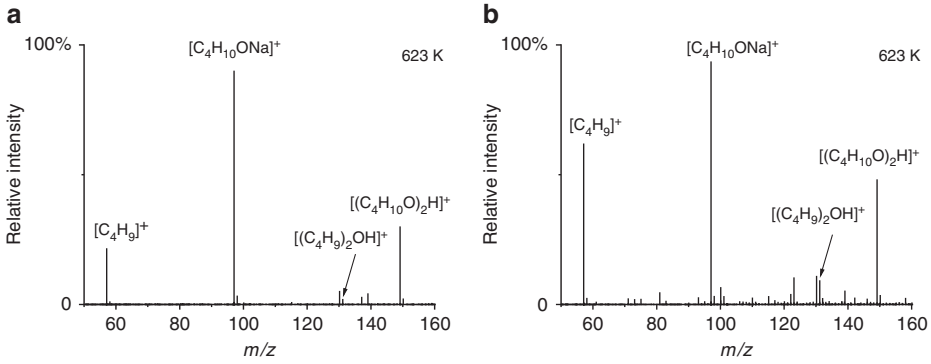

Fig. 2 The MS spectra of cationic species in butanol dehydration. Heterogeneous catalytic reaction of 1-butanol (**a**) and 2-butanol (**b**) dehydration was performed on γ-Al_2O_3 at 623 K. The resolution of MS was set as 30,000 for full MS scans, and no ionization voltage was applied. The sodium in $[C_4H_{10}ONa]^+$ may come from the γ-Al_2O_3 catalyst (see Supplementary Table 1 for elemental analysis)

Although 1-butanol was applied, the unimolecular dehydration of butene formation was still the major process in the γ-Al_2O_3 heterogeneous catalysis and the abundance of 1-butanol dehydration cationic species ($[C_4H_9]^+$) was about ten times higher than the protonated 1-butanol ether ($[(C_4H_9)_2OH]^+$) (Fig. 2a), which was highly consistent with the previous reports on investigating the olefin and ether synthesis rates of butanol on γ-Al_2O_3[19,20]. The high abundance of unimolecular dehydration cationic species $[C_4H_9]^+$ implied that the C_β–H bond cleavage is the rate-determining step (RDS) of the unimolecular dehydration process. The above results were also validated by the previous reports on studying the kinetic isotope effects in the olefin formation from butanols[20,21]. Our results exhibited that the catalytic reaction temperature was crucial to 1-butanol dehydration on γ-Al_2O_3, and the abundances of cationic species generated within heterogeneous catalysis were exponentially increased along with the reaction temperature increasing (Supplementary Figure 2). However, many other cationic species of unsaturated olefins (or aromatics) and alkoxy (or aldehyde) derivatives were further observed at 723 K with a relatively low abundance (Supplementary Figure 2 and Supplementary Data 1), which might be attributed to the tandem catalytic reactions of 1-butanol dehydration products on γ-Al_2O_3, such as isomerization, polymerization, and cracking[22–24].

Then, 2-butanol was injected into the micro catalytic reactor packed with γ-Al_2O_3 at 623 K. The cationic species generated within the 2-butanol dehydration process was similar to 1-butanol and $[(C_4H_{10}O)_2H]^+$, $[(C_4H_9)_2OH]^+$, and $[C_4H_9]^+$ were also observed. Compared with 1-butanol, the relative abundance of unimolecular dehydration cationic species $[C_4H_9]^+$ was significantly improved in 2-butanol dehydration at identical conditions (Fig. 2b), which could be attributed to the secondary carbeniums being more stable than the primary ones. Thus, the olefin formation process is more preferred in the 2-butanol catalytic dehydration[19,20]. Further, more cationic species of unsaturated olefins (or aromatics) and alkoxy (or aldehyde) derivatives were observed at a lower temperature than 1-butanol catalytic dehydration (Fig. 2 and Supplementary Data 1). This could be attributed to the fact that more olefins are generated in the 2-butanol catalytic dehydration process as described above.

Methanol dehydration on H-Beta and H-ZSM5. The above results clearly demonstrated that our strategy can successfully detect the short-lived cationic species generated in the relatively simple heterogeneous catalysis system of butanol dehydration on γ-Al_2O_3. Then, a much more complex heterogeneous catalysis system of methanol dehydration on acidic zeolites was investigated. First, methanol was injected into the micro catalytic reactor packed with H-Beta[25] and hundreds of cationic species with mono positive charge were clearly detected in the MS at 623 K (Fig. 3a). The elemental composition of 477 ionic compounds was feasibly determined as high mass accuracy was achieved by an Orbitrap analyzer (Supplementary Data 1). The high mass resolution of MS was essential to discriminate different cationic species with molecular weights close to each other. For example, the mass of $[C_8H_9O_4]^+$, $[C_{12}H_9O]^+$, $[C_9H_{13}O_3]^+$, $[C_{13}H_{13}]^+$, $[C_{10}H_{17}O_2]^+$, and $[C_{11}H_{21}O]^+$ are 169.05, 169.07, 169.09, 169.10, 169.12, and 169.16 Da, respectively, which cannot be discriminated by common quadrupole and ion trap MS but are clearly discriminated in our study (Supplementary Figure 4). To further validate the reliability of the assigned elemental composition for these cationic species, we utilized $^{13}CH_3OH$ to replace CH_3OH for the reaction at identical conditions. Then, the heavy isotopic forms of about 70% cationic species could be feasibly observed (Table 1 and Supplementary Data 1). If we consecutively inject 100 μL of H_2O three times to deactivate the acidic zeolite followed by CH_3OH injection, almost all cationic species generated within the reaction were significantly decreased accordingly (Supplementary Figure 5). These cationic species could mainly be assorted into two categories, including unsaturated olefins (or aromatics) $[C_nH_{2n-3}]^+$, $[C_nH_{2n-5}]^+$, $[C_nH_{2n-7}]^+$, $[C_nH_{2n-9}]^+$, $[C_nH_{2n-11}]^+$, and so on, and unsaturated alkoxy (or aldehyde) derivatives $[C_nH_{2n+1}O_{1,2}]^+$, $[C_nH_{2n-1}O_{1,2,3}]^+$, $[C_nH_{2n-3}O_{1,2,3}]^+$, $[C_nH_{2n-5}O_{1,2,3}]^+$, $[C_nH2_{n-7}O_{1,2,3,4}]^+$, and so on (Fig. 3a, Table 1, and Supplementary Data 1). The generation of olefins (or aromatics) cationic species can be explained by conventional paring and side-chain reaction routes for methanol to hydrocarbons conversion[10,26–28]. The mass of important cationic intermediates 1,3-dimethylcyclopentenyl ($[C_7H_{11}]^+$), pentamethylcyclopentenyl ($[C_{10}H_{17}]^+$), 1,1,2,4,6-pentamethylbenzenium ($[C_{11}H_{17}]^+$), heptamethylcyclopentenyl ($[C_{12}H_{21}]^+$), and heptamethylbenzenium ($[C_{13}H_{21}]^+$) previously identified by in situ solid-state NMR were all observed in our results. However, the unsaturated alkoxy (or aldehyde) cationic species were rarely reported previously.

It is widely recognized that methanol is firstly dehydrated to generate dimethyl ether (DME), followed by formation of other hydrocarbons. However, the detail reaction route of DME generation is still controversial[29]. We observed the protonated methanol dimer with a relatively high abundance (Fig. 3a), indicating that protonated methanol dimer widely existed in methanol to hydrocarbons conversion. This might be experimental evidence that two methanol molecules are adsorbed together and reacted simultaneously to form DME, which is also the preferred route due to its lower activation barrier[30]. Although previous reports speculated the formation of trimethyloxonium in

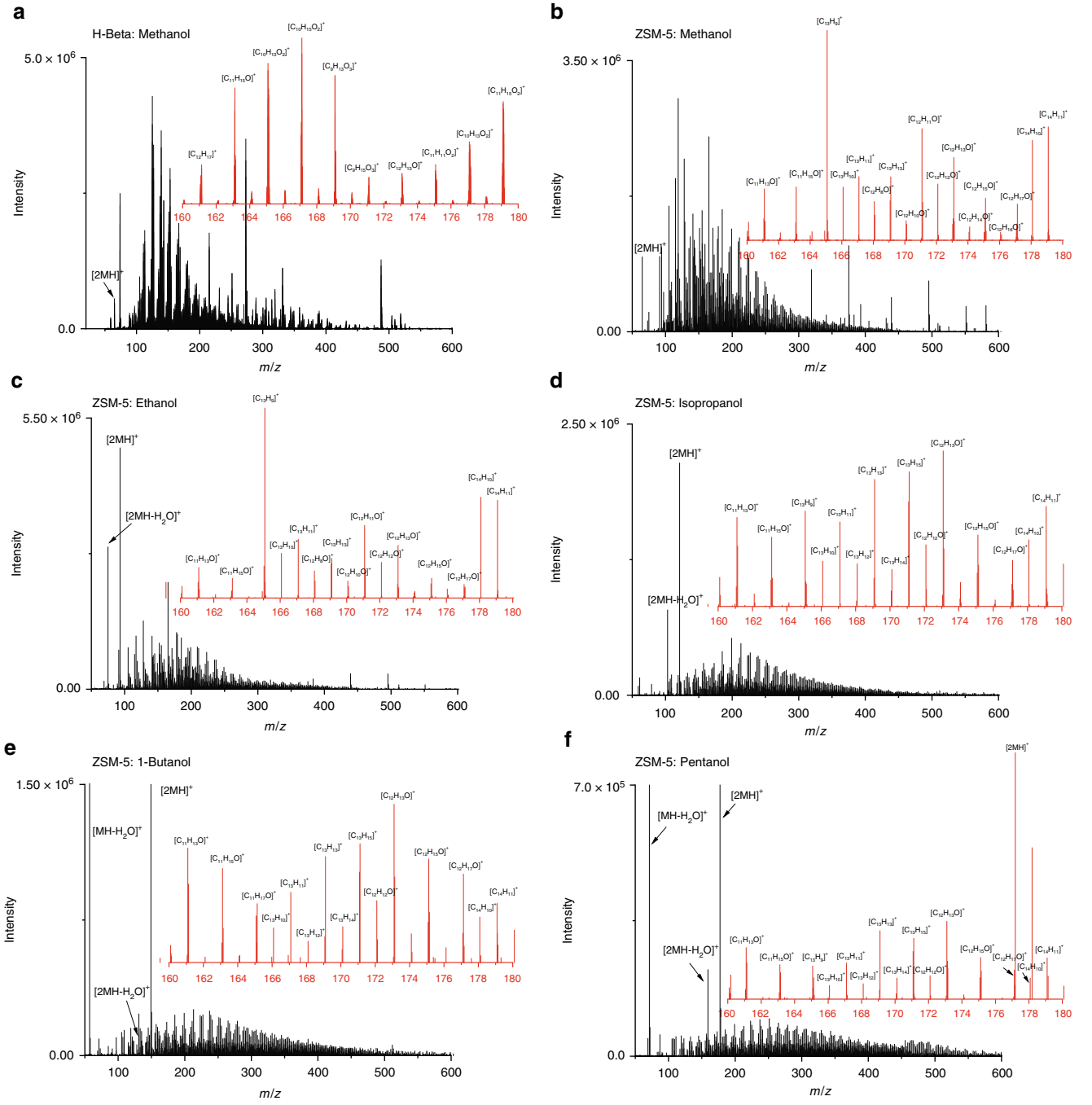

Fig. 3 The MS spectra of short-lived cationic species. Short-chain alcohols dehydration was performed on acidic zeolites: H-Beta with methanol (**a**), and H-ZSM5 with methanol (**b**), ethanol (**c**), isopropanol (**d**), butanol (**e**), and pentanol (**f**). The mass range 160–180 was enlarged and put on top of the figures with elemental compositions of the main peaks (red). Alcohols were injected at 10 μL/s and the reaction temperature was kept at 623 K. The resolution was set as 30,000 for full MS scans. $[2MH]^+$, $[2MH\text{-}H_2O]^+$, and $[MH\text{-}H_2O]^+$ were protonated dimer, dehydrated dimer, and dehydrated monomer of the reacted alcohol

the first C–C formation[31], we have not observed it, which is validated by the result obtained from solid-state NMR[32]. In the reaction temperature investigation, the types and abundance of cationic species were both increased along with improving the reaction temperature from 373 to 623 K (Supplementary Figure 6 and Supplementary Figure Data 1). Although neither olefins nor DME was observed at 373 K in solid-state NMR[33], we found that parts of the alkoxy (or aldehyde) cationic species were already generated at this temperature with low abundance, including $[C_nH_{2n-3}O_2]^+$, $[C_nH_{2n-5}O_{1,2,3}]$, and $[C_nH_{2n-7}O_2]^+$ ($n = 5$–11), which further demonstrated the high detection sensitivity of our strategy. The olefins and aromatics cationic species began to appear at 423 K, such as $[C_5H_7]^+$, $[C_7H_7]^+$, $[C_8H_9]^+$, $[C_8H_{11}]^+$, and $[C_9H_9]^+$. At 523 K, most of the cationic species could be already observed with a relatively lower intensity compared with 623 K. Therefore, the alkoxy (or aldehyde) cationic species widely existed in methanol dehydration at our reaction condition and could be generated at a much lower reaction temperature than olefins and aromatics cationic species.

We further packed a strong acidic zeolite H-ZSM5[34] into the micro catalytic reactor for investigating the short-lived cationic species generation in methanol dehydration at 623 K. Although

Table 1 The detailed information of high-abundant cationic species in methanol dehydration on H-Beta

Formula	M_{expC12}	$M_{theroC12}$	RE (ppm)	M_{expC13}	$\Delta M_{(C13-C12)}$
$[C_5H_9]^+$	69.07041	69.07043	−0.3	74.08737	5.01697
$[C_4H_9O]^+$	73.06536	73.06534	0.2	77.07941	4.01406
$[C_3H_7O_2]^+$	75.04458	75.04461	−0.4	78.05479	3.01022
$[C_6H_7]^+$	79.05478	79.05478	0.0	85.07511	6.02034
$[C_7H_7]^+$	91.05482	91.05478	0.4	98.07829	7.02348
$[C_6H_6O]^+$	94.04192	94.04187	0.5	100.06201	6.02010
$[C_6H_9O]^+$	97.06541	97.06534	0.7	103.08560	6.02020
$[C_6H_{11}O]^+$	99.08103	99.08099	0.4	105.10121	6.02019
$[C_8H_9]^+$	105.07050	105.07043	0.7	113.09725	8.02676
$[C_8H_{11}]^+$	107.08619	107.08608	1.0	115.11290	8.02672
$[C_7H_9O]^+$	109.06539	109.06534	0.4	116.08874	7.02336
$[C_7H_{11}O]^+$	111.08110	111.08099	0.9	118.10487	7.02378
$[C_6H_{11}O_2]^+$	115.07598	115.07591	0.6	121.09618	6.02021
$[C_9H_9]^+$	117.07046	117.07043	0.3	126.10051	9.03006
$[C_9H_{11}]^+$	119.08610	119.08608	0.2	128.11628	9.03019
$[C_8H_9O]^+$	121.06534	121.06534	0.0	129.09212	8.02679
$[C_7H_9O_2]^+$	125.06032	125.06026	0.5	132.08355	7.02324
$[C_{10}H_8]^+$	128.06271	128.06260	0.8	138.09607	10.03337
$[C_{10}H_9]^+$	129.07048	129.07043	0.4	139.10412	10.03365
$[C_7H_{13}O_2]^+$	129.09165	129.09156	0.7	ND	
$[C_9H_{11}O]^+$	135.08110	135.08099	0.8	144.11127	9.03018
$[C_8H_9O_2]^+$	137.06026	137.06026	0.0	145.08694	8.02669
$[C_{11}H_9]^+$	141.07045	141.07043	0.1	152.10786	11.03742
$[C_7H_{11}O_3]^+$	143.07095	143.07082	0.9	150.09388	7.02294
$[C_{10}H_8O]^+$	144.05761	144.05752	0.6	154.09109	10.03349
$[C_{11}H_{15}]^+$	147.11749	147.11738	0.7	158.15426	11.03678
$[C_9H_{11}O_2]^+$	151.07593	151.07591	0.1	160.10609	9.03017
$[C_{12}H_8]^+$	152.06273	152.06260	0.8	164.10290	12.04018
$[C_{12}H_{11}]^+$	155.08615	155.08608	0.5	167.12626	12.04012
$[C_8H_{13}O_3]^+$	157.08661	157.08647	0.9	ND	
$[C_{11}H_{11}O]^+$	159.08105	159.08099	0.3	170.11778	11.03674
$[C_{11}H_{13}O]^+$	161.09674	161.09664	0.6	172.13341	11.03668
$[C_{11}H_{15}O]^+$	163.11243	163.11229	0.8	174.14904	11.03662
$[C_{13}H_9]^+$	165.07054	165.07043	0.7	178.11421	13.04368
$[C_{12}H_{13}O]^+$	173.09681	173.09664	1.0	185.13674	12.03994

The exact mass and elemental composition of 35 high-abundant cationic species were obtained in methanol dehydration on H-Beta at 623 K. $^{13}CH_3OH$ was utilized to replace CH_3OH for validation M_{expC12} and M_{expC13} experimental mass of cationic species generated with CH_3OH and $^{13}CH_3OH$ on H-Beta, respectively, and $M_{theroC12}$ theoretical mass, RE relative error, and $\Delta M_{(C13-C12)}$ mass incensement by using $^{13}CH_3OH$ to replace CH_3OH

the general categories of cationic species were similar to those observed in H-Beta experiments, H-ZSM5 exhibited a much higher activity and selectivity in producing olefins (or aromatics) cationic species. Within the mass range *m/z* 50–200, the number of cationic species of olefins (or aromatics) were increased to 28% and the corresponding total MS signal intensity was enhanced more than three times. In contrast, both the types and abundance of alkoxy (or aldehyde) cationic species were greatly suppressed in H-ZSM5 catalytic reactions (Fig. 3a, b, Supplementary Figure 7, and Supplementary Data 1). The most abundant cationic species were usually olefins or alkoxy cations with only one oxygen atom in H-ZSM5 reactions, which was significantly different from H-Beta that alkoxy cations with two or more oxygen atoms were always the most abundant ones. The cationic species with more than three oxygen atoms were nearly absent in H-ZSM5 reactions. Obviously, the formation of cationic species is directly related to the activity and selectivity of an acidic zeolite catalyst, and H-ZSM5 can greatly reduce the overall oxygen contents of cationic species.

Short-chain alcohol dehydration on H-ZSM5. Then, ethanol, isopropanol, butanol, and pentanol were injected into the micro catalytic reactor packed with H-ZSM5 at 623 K. The chemical compositions of the cationic species observed in catalytic dehydration of these alcohols were highly similar, which demonstrated that similar hydrocarbon pools might be formed during the catalytic dehydration of short-chain alcohols (Fig. 3a–f and Supplementary Data 1). Although the absolute MS signal intensity of cationic species was decreased along with the increase of alcohols carbon numbers, the selectivity for producing olefins (or aromatics) cationic species was improved accordingly, concomitant to the types and abundance of alkoxy (or aldehyde) cationic species that were further suppressed, especially for the ones with multi-oxygen atoms (Fig. 3 and Supplementary Figure 7). This can be attributed to the C–C bonds that already existed in alcohols with multi carbon atoms, which are easily dehydrated to form olefins (the corresponding protonated alcohol dimers, dehydrated dimers, and dehydrated monomers were all observed). Thus, the overall oxygen contents of cationic species are decreased for alcohols with multi carbon atoms. However, coke formation on zeolite surfaces was more serious for alcohols with more carbon atoms, which might be the reason of MS signal intensity decreasing for the cationic species.

Discussion

It is well known that the cationic species are widely involved in the process of catalytic dehydration of short- chain alcohols, yet few cationic species have been directly observed by the experiment up to now due to the lack of an efficient detection tool[19,20,35,36]. We integrated a micro catalytic reactor packed with a solid catalyst onto the Orbitrap MS ion inlet, allowing the cationic species generated in heterogeneous catalysis to

simultaneously come into the MS as fast as possible for high-throughput detection. This strategy can significantly enhance the probability for detecting the short-lived cationic species. Butanol dehydration on solid γ-Al_2O_3 is a widely studied heterogeneous catalytic reaction, yet the mechanism is still controversial[20,21,35,37]. Our results suggest that olefin formation is the major process in butanol dehydration on γ-Al_2O_3, and the C_β–H bond cleavage is the RDS in the unimolecular dehydration process. There are both hydroxyl groups and Lewis acid sites on the γ-Al_2O_3 surface. Thus, the cationic species $[C_4H_9]^+$ might be generated through two different pathways by interacting with the surface hydroxyl groups and Lewis acid sites (Supplementary Figure 8).

Both the reactants and solid catalysts play crucial roles in the heterogeneous catalytic reaction. In our study, the 2-butanol could produce relatively more cationic species $[C_4H_9]^+$ than 1-butanol due to the secondary carbeniums that are more stable and unimolecular dehydration more likely occurred. More interestingly, the cationic species generated in acidic zeolites catalyzed experiments were far beyond our expectations, and hundreds of unsaturated olefins or alkoxy cations were clearly observed. The generation of these cationic species might be attributed to the formation of a complex hydrocarbon pool, and the cationic intermediates produced onto the zeolite surface come into the gas phase and then ionize or react with the mixture of hydrocarbons and unreacted alcohols[38]. We further injected pentene or phenyl olefins into the micro catalytic reactor packed with H-ZSM5 to investigate if the cationic species could be formed by protonation of neutral olefin products onto the catalyst surface. However, no cationic species could be observed at these conditions with olefins as reactants in our system (data not shown). Thus, the cationic species are generated by the catalytic process of alcohol dehydration, not by the protonation of olefins on acidic zeolites or MS heating capillary.

Our key findings are as follows: first, the carbon chains of cationic species generated in the alcohol-to-hydrocarbon processes are gradually propagating from several to over 20 carbons and highly unsaturated polyaromatic rings must be formed; second, the alkoxy (or aldehyde) cationic species widely exist within the alcohol-to-hydrocarbon conversion, which can be generated at a lower reaction temperature compared to olefins and aromatics cationic species; third, the acidic zeolite with higher activity and selectivity for olefins (or aromatics) production (H-ZSM5) can significantly decrease the overall oxygen contents of cationic species; fourth, very similar cationic species were observed for alcohol reactants from C1 to C5, which means that carbon chain propagation, isomerization, and cracking should be common in the alcohol-to-hydrocarbon conversion. Overall, the observed cationic species by our strategy are directly related to the catalytic activity and selectivity of alcohol dehydration processes. Hence, we believe that this method exhibits great potential in both catalyst screening and reaction condition refinement in the future.

In summary, a micro catalytic reactor packed with a solid catalyst was integrated onto the ion inlet of Orbitrap MS, which seems suitable for detecting the short-lived cationic species generated in heterogeneous catalysis of alcohol dehydration due to its high speed, high sensitivity, and high throughput. This strategy is complementary to conventional in situ techniques for active species characterization on solid catalysts and might be helpful for investigating the heterogeneous catalytic reactions related with cationic species.

Methods

Materials. Γ-Al_2O_3 (product number 267740), 1-butanol, and 2-butanol were obtained from Sigma (St. Louis, MO, USA). PEEK tubing and sleeves were obtained from Upchurch Scientific (Oak Harbor, WA, USA). Fused silica capillaries with 75 μm i.d. were purchased from Polymicro Technologies (Phoenix, AZ, USA). The element concentration of γ-Al_2O_3 was characterized by X-ray fluorescence spectrometer (Magix 601) and provided in Supplementary Table 1.

Cationic species detection. The integrated micro catalytic reactor was fabricated by stainless steel, and it was designed with a reaction chamber (1 mm i.d. × 8 mm) for γ-Al_2O_3, H-Beta[25], or H-ZSM5[34] packing and a pre-heat chamber (2 mm i.d. × 10 mm) for alcohol pre-heating and gasifying (Fig. 1 and Supplementary Figure 1). The reaction chamber was fabricated within the connection fittings of a stainless-steel union and was directly integrated onto the ion transfer capillary inlet of Orbitrap MS. The temperature of the micro catalytic reactor for dehydration catalytic reaction could be adjusted from 373 to 723 K by controlling the temperature of MS ion transfer capillary. The pre-heat chamber was fabricated within the body of a stainless-steel union. The stainless-steel fittings on the other side of the union were connected with a 75 μm i.d. capillary for alcohol reactant introduction. γ-Al_2O_3, H-Beta, and H-ZSM5 were activated by 873-K calcination for at least 4 h before use. The main characteritics of these catalysts were provided in Supplementary Table 1. Before alcohol injection, the system gas pressure of the micro catalytic reactor was about 100 Pa because it was directly connected to the MS high vacuum system. After alcohol injection (10 μL/s), the alcohol reagent could be rapidly gasified due to the high temperature and low gas pressure of the catalytic reactor. Then, the pre-heated alcohol gas flow passed through the packed γ-Al_2O_3 or acidic zeolites bed and directly comes into MS.

Mass spectrometric detection. The MS analysis was performed on LTQ-Orbitrap XL mass spectrometer (Thermo, San Jose, CA, USA) at a resolution of 30,000 and survey full scan MS was acquired from *m/z* 50 to 600. The MS data collection was performed by Xcalibur 2.1.0 (Thermo). The temperature of the ion transfer capillary could be set at between 373 with 723 K according to the requirement of catalytic dehydration reactions. The spray voltage was set at 0 V. One microscan was set for each MS. The target ion setting was 5e5 for the Orbitrap, with a maximum fill-time of 200 ms.

Data availability

The datasets generated and analyzed during the current study are available on the figshare website, DOI: 10.6084/m9.figshare.6176072, or from the corresponding author upon reasonable request.

Received: 20 April 2018 Accepted: 9 August 2018
Published online: 05 September 2018

References

1. Senkan, S. M. High-throughput screening of solid-state catalyst libraries. *Nature* **394**, 350–353 (1998).
2. Wassenaar, J. et al. Catalyst selection based on intermediate stability measured by mass spectrometry. *Nat. Chem.* **2**, 417–421 (2010).
3. Weckhuysen, B. M. Preface: recent advances in the in-situ characterization of heterogeneous catalysts. *Chem. Soc. Rev.* **39**, 4557–4559 (2010).
4. Robbins, D. W. & Hartwig, J. F. A simple, multidimensional approach to high-throughput discovery of catalytic reactions. *Science* **333**, 1423–1427 (2011).
5. Thibault-Starzyk, F. et al. Real-time infrared detection of cyanide flip on silver-alumina NO*x* removal catalyst. *Science* **324**, 1048–1051 (2009).
6. Xu, S. T., Zhang, W. P., Liu, X. C., Han, X. W. & Bao, X. H. Enhanced in situ continuous-flow MAS NMR for reaction kinetics in the nanocages. *J. Am. Chem. Soc.* **131**, 13722–13727 (2009).
7. Stosser, R., Marx, U., Herrmann, W., Jabor, J. K. & Bruckner, A. In situ EPR study of chemical reactions in Q-band at higher temperatures: a challenge for elucidating structure–reactivity relationships in catalysis. *J. Am. Chem. Soc.* **132**, 9873–9880 (2010).
8. Urakawa, A., Maeda, N. & Baiker, A. Space- and time-resolved combined DRIFT and raman spectroscopy: monitoring dynamic surface and bulk processes during NO(x) storage reduction. *Angew. Chem. Int. Ed.* **47**, 9256–9259 (2008).
9. Woertink, J. S. et al. A $[Cu_2O](2+)$ core in Cu-ZSM-5, the active site in the oxidation of methane to methanol. *Proc. Natl. Acad. Sci. USA* **106**, 18908–18913 (2009).
10. Dahl, I. M. & Kolboe, S. On the reaction-mechanism for hydrocarbon formation from methanol over Sapo-34 .1. Isotopic labeling studies of the co-reaction of ethene and methanol. *J. Catal.* **149**, 458–464 (1994).
11. Dahl, I. M. & Kolboe, S. On the reaction mechanism for hydrocarbon formation from methanol over SAPO-34 .2. Isotopic labeling studies of the co-reaction of propene and methanol. *J. Catal.* **161**, 304–309 (1996).
12. Chen, H., Eberlin, L. S., Nefliu, M., Augusti, R. & Cooks, R. G. Organic reactions of ionic intermediates promoted by atmospheric-pressure thermal activation. *Angew. Chem. Int. Ed.* **47**, 3422–3425 (2008).

13. Brown, T. A., Chen, H. & Zare, R. N. Detection of the short-lived radical cation intermediate in the electrooxidation of *N,N*-dimethylaniline by mass spectrometry. *Angew. Chem. Int. Ed.* **54**, 11183–11185 (2015).
14. Brown, T. A., Chen, H. & Zare, R. N. Identification of fleeting electrochemical reaction intermediates using desorption electrospray ionization mass spectrometry. *J. Am. Chem. Soc.* **137**, 7274–7277 (2015).
15. Banerjee, S. & Zare, R. N. Syntheses of isoquinoline and substituted quinolines in charged microdroplets. *Angew. Chem. Int. Ed.* **54**, 14795–14799 (2015).
16. Yan, X. et al. On-line reaction monitoring and mechanistic studies by mass spectrometry: Negishi cross-coupling, hydrogenolysis, and reductive amination. *Angew. Chem. Int. Ed.* **53**, 5931–5935 (2014).
17. Guisnet, M., Costa, L. & Ribeiro, F. R. Prevention of zeolite deactivation by coking. *J. Mol. Catal. A* **305**, 69–83 (2009).
18. Serrano-Ruiz, J. C. & Dumesic, J. A. Catalytic routes for the conversion of biomass into liquid hydrocarbon transportation fuels. *Energy Environ. Sci.* **4**, 83–99 (2011).
19. Shi, B. C. & Davis, B. H. Alcohol dehydration: mechanism of ether formation using an alumina catalyst. *J. Catal.* **157**, 359–367 (1995).
20. Kang, M. J., DeWilde, J. F. & Bhan, A. Kinetics and mechanism of alcohol dehydration on gamma-Al_2O_3: effects of carbon chain length and substitution. *ACS Catal.* **5**, 602–612 (2015).
21. Knözinger, H. & Scheglila, A. The dehydration of alcohols on alumina: XII. Kinetic isotope effects in the olefin formation from butanols. *J. Catal.* **17**, 252–263 (1970).
22. Rahimi, N. & Karimzadeh, R. Catalytic cracking of hydrocarbons over modified ZSM-5 zeolites to produce light olefins: a review. *Appl. Catal. A* **398**, 1–17 (2011).
23. Haibach, M. C., Kundu, S., Brookhart, M. & Goldman, A. S. Alkane metathesis by tandem alkane-dehydrogenation-olefin-metathesis catalysis and related chemistry. *Acc. Chem. Res.* **45**, 947–958 (2012).
24. Jiao, F. et al. Selective conversion of syngas to light olefins. *Science* **351**, 1065–1068 (2016).
25. Zhang, M. et al. Methanol to hydrocarbons reaction over Hβ zeolites studied by high resolution solid-state NMR spectroscopy: carbenium ions formation and reaction mechanism. *J. Catal.* **335**, 47–57 (2016).
26. Arstad, B., Nicholas, J. B. & Haw, J. F. Theoretical study of the methylbenzene side-chain hydrocarbon pool mechanism in methanol to olefin catalysis. *J. Am. Chem. Soc.* **126**, 2991–3001 (2004).
27. Li, J. Z. et al. Observation of heptamethylbenzenium cation over SAPO-type molecular sieve DNL-6 under real MTO conversion conditions. *J. Am. Chem. Soc.* **134**, 836–839 (2012).
28. Xu, S. T. et al. Direct observation of cyclic carbenium ions and their role in the catalytic cycle of the methanol-to-olefin reaction over chabazite zeolites. *Angew. Chem. Int. Ed.* **52**, 11564–11568 (2013).
29. Blaszkowski, S. R. & van Santen, R. A. Theoretical study of C–C bond formation in the methanol-to-gasoline process. *J. Am. Chem. Soc.* **119**, 5020–5027 (1997).
30. Blaszkowski, S. R. & van Santen, R. A. The mechanism of dimethyl ether formation from methanol catalyzed by zeolitic protons. *J. Am. Chem. Soc.* **118**, 5152–5153 (1996).
31. Olah, G. A. et al. Onium ylide chemistry. 1. Bifunctional acid base-catalyzed conversion of heterosubstituted methanes into ethylene and derived hydrocarbons—the onium ylide mechanism of the C1–C2 conversion. *J. Am. Chem. Soc.* **106**, 2143–2149 (1984).
32. Munson, E. J., Kheir, A. A., Lazo, N. D. & Haw, J. F. In situ solid-state NMR study of methanol-to-gasoline chemistry in zeolite H-ZSM5. *J. Phys. Chem.* **96**, 7740–7746 (1992).
33. Seiler, M., Schenk, U. & Hunger, M. Conversion of methanol to hydrocarbons on zeolite H-ZSM5 investigated by in situ MAS NMR spectroscopy under flow conditions and on-line gas chromatography. *Catal. Lett.* **62**, 139–145 (1999).
34. Zhang, M. et al. Methanol conversion on ZSM-22, ZSM-35 and ZSM-5 zeolites: effects of 10-membered ring zeolite structures on methylcyclopentenyl cations and dual cycle mechanism. *RSC Adv.* **6**, 95855–95864 (2016).
35. Christiansen, M. A., Mpourmpakis, G. & Vlachos, D. G. Density functional theory-computed mechanisms of ethylene and diethyl ether formation from ethanol on gamma-Al_2O_3(100). *ACS Catal.* **3**, 1965–1975 (2013).
36. DeWilde, J. F., Chiang, H., Hickman, D. A., Ho, C. R. & Bhan, A. Kinetics and mechanism of ethanol dehydration on gamma-Al_2O_3: the critical role of dimer inhibition. *ACS Catal.* **3**, 798–807 (2013).
37. Larmier, K. et al. Mechanistic Investigation of isopropanol conversion on alumina catalysts: location of active sites for alkene/ether production. *ACS Catal.* **5**, 4423–4437 (2015).
38. Wilson, P. F. et al. Reactions of CH_3OCH^{2+} with hydrocarbons O, N and S compounds: applications for chemical ionization in selected ion flow tube studies. *J. Am. Soc. Mass Spectrom.* **13**, 1028–1033 (2002).

Acknowledgements

The authors greatly appreciated Dr. Shutao Xu for providing acidic zeolites H-Beta (Si/Al = 24) and H-ZSM5 (Si/Al = 19), Dr. Keyong Hou for help in fabricating the micro catalytic reactor, and Dr. Shengjun Huang for the helpful discussion. Financial supports are gratefully acknowledged from the China State Key Research Grant (2016YFF0200504), the National Natural Science Foundation of China (21675152), the Youth Innovation Promotion Association CAS (2014164), and a grant from DICP (ZZBS201603) to F.W.

Author contributions

F.W. conceived the research, designed the experiments, and wrote the manuscript. Z.L performed MS data analysis. G.W. performed part of the MS experiments of butanol dehydration.

Additional information

Supplementary information accompanies this paper at https://doi.org/10.1038/s42004-018-0053-8.

Competing interests: The authors declare that they have no competing interests.

Reprints and permission information is available online at http://npg.nature.com/reprintsandpermissions/

Publisher's note: Springer Nature remains neutral with regard to jurisdictional claims in published maps and institutional affiliations.